ACERP: Vol. 3, No. 2, (Spiring 2017) 7-13

Advanced Ceramics Progress

Research Article

Journal Homepage: www.acerp.ir

Fabrication and Structural Characterization of Se-Ge Chalcogenide Glasses by Means of Melt Quenching Technique

M. Ghayebloo[a], M. Rezvani[a]*, M. Tavoosi[b]

[a]*Department of Materials Science and Engineering, University of Tabriz, Tabriz, Iran.*
[b]*Department of Materials Engineering, Malek-Ashtar University of Technology (MUT), Tehran, Iran.*

PAPER INFO

Paper history:
Received 10 December 2016
Accepted in revised form 03 October 2017

Keywords:
Chalcogenide glass
Se-Ge
IR transmittance

ABSTRACT

In this study, the structural and optical characterization of Se-Ge alloys during melt quenching technique have been investigated. For this purpose, five different samples of $Se_{100-x}Ge_x$ (x= 10, 20, 30, 40, 50) were prepared by conventional melt quenching in quartz ampoule. The produced samples were characterized using X-ray diffraction (XRD), Scanning Electron Microscopy (SEM), Differential Scanning Calorimetry (DSC), Fourier Transform Infrared Spectroscopy (FTIR), IR Variable Angle Spectroscopic Ellipsometry (IR-VASE) and Raman Spectroscopy. The results showed that the glass forming ability of $Se_{70}Ge_{30}$ and $Se_{50}Ge_{50}$ is so low and the structures of these alloys after quenching are combination of amorphous, $GeSe_2$ and Ge_2Se_3 compounds. Although the structure of as-prepared $Se_{90}Ge_{10}$, $Se_{80}Ge_{20}$ and $Se_{60}Ge_{40}$ is fully amorphous, only $Se_{60}Ge_{40}$ shows IR transmittance (with transmittance higher than 55% between 0.8-11 μm). The refractive index of this glass was in the range of 2.0 to 2.6 and it was decreased with increasing the wavelength. The Fermi energy, Urbach energy, indirect and direct band gaps values of $Se_{60}Ge_{40}$ glass were estimated about 0.3879, 0.1526, 1.345 and 1.28 eV, respectively.

1. INTRODUCTION

Chalcogenide glasses have attracted the attention of many investigators due to the fact that they are potential candidates for applications in infrared optics, photonics devices, reversible optical recording, memory switching, inorganic photoresists and anti-refraction coatings. The main applications of this kind of glasses are for transmission in infrared (IR) range for optical communications systems [1]. Selenium is an excellent glass former, however, pure Se has disadvantages such as low physical (glass forming ability, optical properties and etc.) and mechanical properties [2]. It is well-known that the amorphous forming composition of Ge–Se alloys ranges from pure Se to Ge_3Se_4 by a rapidly melt-quenching method. It has become apparent that the 4(Ge)–2(Se) folded structural model with covalent nature is applicable for amorphous samples in this composition range. Crystalline $GeSe_2$ is constructed by $GeSe_{4/2}$ tetrahedral units connecting each other at the corners or edges, in which a central Ge is covalently bonded to four Se. The importance of optical methods to the study of local structure in binary chalcogenide glasses has been demonstrated recently for the Ge_xSe_{1-x} system [3, 4].

Although there are a lot of studies about the formation and characterization of Se-Ge chalcogenide glasses, the formation and characterization of bulk Se-Ge glasses has not been properly investigated. So, in this study, the structural and optical characterizations of $Se_{100-x}Ge_x$ (x= 10, 20, 30, 40, 50) has been investigated. The exact effect of Ge on optical properties of bulk Se-Ge glasses and the relation between network connectivity and optical properties of these alloys is another issue that is studied in this work.

2. MATERIALS, METHOD

Bulk $Se_{100-x}Ge_x$ (x= 10, 20, 30, 40, 50) samples were prepared through conventional melt quenching technique using high purity Se (Changsha Santech material, 99.99% purity) and Ge (Changsha Santech material, 99.999% purity) elements. Pure Mg element (Merck, 99.99% purity) was also used as gathering material. About 20 g of each batch was transferred to a high purity quartz ampoule (with internal diameter of about 11 mm and cleaned with 0.4%HF), evacuated under vacuum and then sealed. The prepared samples were homogenized at 900°C for 8 h in a rocking furnace and then they were subsequently quenched at quenching

*Corresponding Author's Email: M_Rezvani@tabrizu.ac.ir (M. Rezvani)

media at different temperatures. The quenching conditions for each sample are presented in Table 1. After that, as-prepared samples were annealed at about 20°C below glass transition temperature for 4 h and slowly cooled down to room temperature.

TABLE 1. The quenching media and temperature for formation of bulk Ge-Se samples

S.N.	Composition	Quenching media	Quenching Temp. (°C)
Sample 1	$Se_{90}Ge_{10}$	Oil Bath	50
Sample 2	$Se_{80}Ge_{20}$	Oil Bath	100
Sample 3	$Se_{70}Ge_{30}$	Salt Bath	240
Sample 4	$Se_{60}Ge_{40}$	Salt Bath	240
Sample 5	$Se_{50}Ge_{50}$	Salt Bath	240

XRD technique, using a diffractometer with Cu-K_α radiation (λ= 0.15406 nm; 40 kV; Philips PW3710) was employed to follow the structural changes of the specimens (step size: 0.05°; time per step: 1sec.). The structure of the as-prepared samples was investigated by Field Emission Scanning Electron Microscopy (MIRA3 FEG-SEM) at an accelerating voltage of 20kV. Differential Scanning Calorimetry was also conducted to study the thermal behavior of produced samples using the DTG-60AH Shimadzu calorimeter. The samples were placed in Al_2O_3 pans and heated in dynamic argon atmosphere up to 550°C at a heating rate of 10°C/min. The Raman spectra were obtained using a Renishaw In via Raman Spectrometer equipped with a LD laser with the excitation wavelength of 785 nm. The excitation power applied to the measurement is approximately 5 mW. IR Variable Angle Spectroscopic Ellipsometry (IR-VASE, J. A. Woollam Co., Lincoln, NE) was used to measure the linear refractive indices in which the angles of incidence were 70 and 75°. Optical properties of the produced samples were also measured using FT-IR spectrometer (Bruker Tensor 27) in wavelength range of 2.5-17.5 μm and using UV-VIS-NIR spectrometer (Shimadzu UV3100) in wavelength range of 600-2500 nm.

3. RESULT AND DISCUSSION

The glass forming ability (GFA) of one composition directly depends on the reduced glass transition temperature ($T_{rg}=T_g/T_l$; where T_g is glass transition temperature and T_l is liquids temperature) [5]. Turnbull [6] proposed that, the glass forming ability can be increased with increasing T_{rg}. Considering this point, the alloys near to eutectic composition (with lower T_l) have the highest and the alloys near to peritectic reactions (with higher T_l) have the lowest glass forming ability. According to the equilibrium phase diagram of Se-Ge system [7], in selenium rich sides, two eutectic (212°C, 93 at.% of Se and 583°C, 56 at.% of Se) and two peritectic reactions (742°C, 33.33 at.% of Se and 675°C, 50 at.% of Se) can be detected [7]. So, different samples in this work have different abilities in forming glassy phase. For better understanding, the structural and optical investigations of the samples prepared in this work were presented in two separated parts: Se-$GeSe_2$ ($Se_{90}Ge_{10}$, $Se_{80}Ge_{20}$ and $Se_{70}Ge_{30}$) and GeSe-$GeSe_2$ ($Se_{60}Ge_{40}$ and $Se_{50}Ge_{50}$) subsystems.

3.1. $GeSe_2$-Se subsystem

The XRD patterns of $Se_{90}Ge_{10}$, $Se_{80}Ge_{20}$ and $Se_{70}Ge_{30}$ as-prepared samples are presented in Fig. 1. According to these XRD patterns, the microstructure of $Se_{90}Ge_{10}$ and $Se_{80}Ge_{20}$ as-prepared samples are fully amorphous and there is not any evidence of crystalline phases in these specimens. Based on DSC heating traces (Fig. 2), the glass transition temperature of these two calcogenide glasses was estimated as about 96 and 170°C, respectively, which are in agreement with Guin and et al. report [8]. As it can be seen, the glass transition temperature of these specimens increases by increasing the Ge contents. In fact, by adding Ge atoms to Se network, two main phenomena occur:

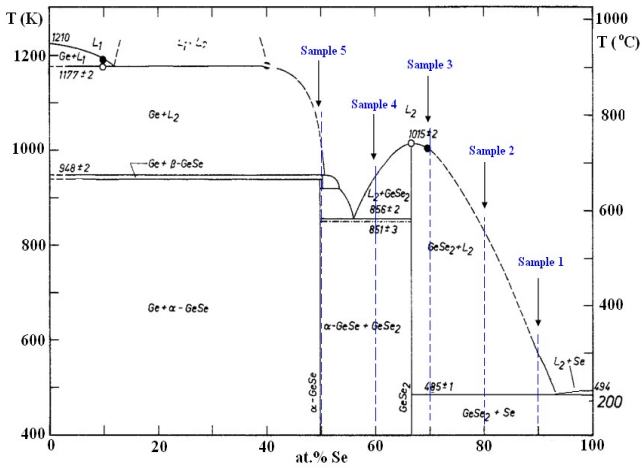

Figure 1. The XRD patterns of $Se_{90}Ge_{10}$, $Se_{80}Ge_{20}$ and $Se_{70}Ge_{30}$ as-prepared samples

1- Increasing the network connectivity; Based on Fig. 3, as the germanium content increases from 10 to 30 at.%, the Se-Se chain bonds decreases, and the Se-Ge bonds with two-fold coordination around selenium and four-fold coordination around germanium increases, progressively. This point illustrates that, the network connectivity (former) is increased by enhancement of the Ge content [9-10].

2- Increasing the bonding energy; By replacement of weaker Se-Se bonding (bonding energy of about 184 kJ/mol [10]) with stronger Ge-Se bonding (bonding

energy of about 215 kJ/mol [10]), therefore the average bonding energy was increased.

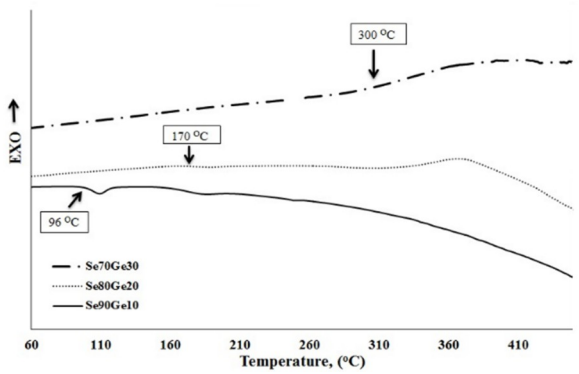

Figure 2. The DSC heating trace of $Se_{90}Ge_{10}$, $Se_{80}Ge_{20}$ and $Se_{70}Ge_{30}$ as-prepared samples in heating rate of 10°C/min

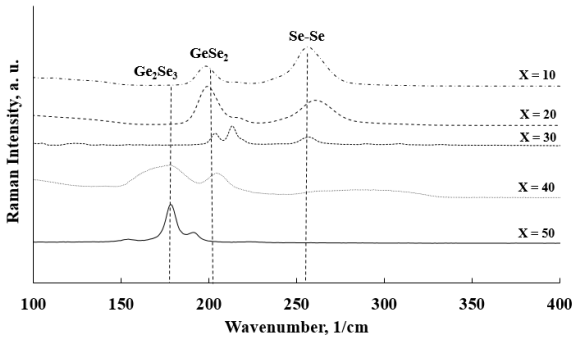

Figure 3. Raman spectra of $Se_{100-x}Ge_x$ (x= 10, 20, 30, 40, 50) as prepared samples

By attention to these points, formation of one glass network with more network connectivity and higher bonding energies are the main reasons of increasing the glass transition temperature with increasing the Ge content. These results are in very good agreement with Popescu et al. [11] report.

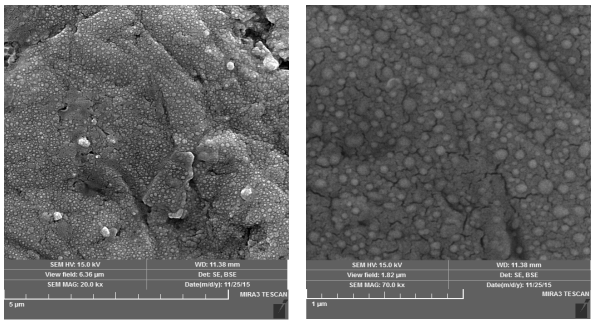

(a) (b)

Figure 4. The SEM micrographs of $Se_{70}Ge_{30}$ as-prepared sample in two magnifications

Besides the $Se_{90}Ge_{10}$ and $Se_{80}Ge_{20}$ samples, the fully amorphous phase is not formed in $Se_{70}Ge_{30}$ sample and the XRD pattern of this specimen (Fig. 1) contains metastable crystalline Ge_3Se_7 [12] peaks which are located in amorphous hallo phase. This phase has an orthorhombic (space group P222) unit cell with a= 6.986 Å, b= 17.808 Å, and c= 12.0761 Å. This result is in agreement with FESEM micrographs of these samples which are presented in Fig. 4.

As it can be observed, the spherical precipitates of Ge_3Se_7 with average particle size of about 70 nm are uniformly dispersed in amorphous matrix. In fact, formation of Ge_3Se_7 metastable phase in $Se_{70}Ge_{30}$ as-prepared sample is the main reason of low glass forming ability of this alloying system. This phase is decomposed to $GeSe_2$ phase during an exothermic reaction at 300°C which is in agreement with Stolen et al. [12] report.

The FTIR spectra of $Se_{90}Ge_{10}$, $Se_{80}Ge_{20}$ and $Se_{70}Ge_{30}$ as-prepared samples are presented in Fig. 5. As it is shown, the IR transmittance of these three samples is near to zero. Although, the formation of Ge_3Se_7 crystalline phase in $Se_{70}Ge_{30}$ specimen is the main reason of low transmittance of this sample, the low IR transmittance of fully amorphous $Se_{90}Ge_{10}$ and $Se_{80}Ge_{20}$ can be attributed to two main reasons:

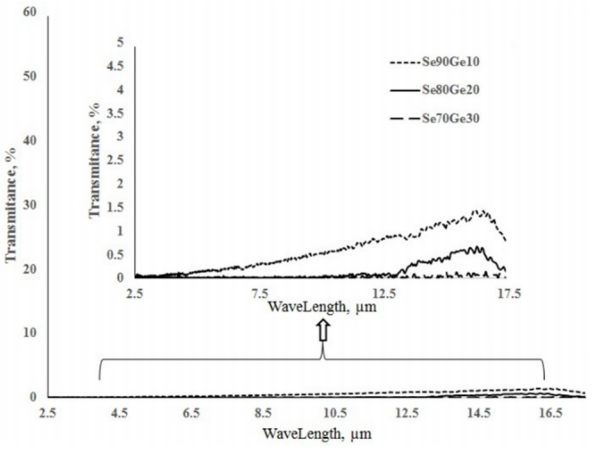

Figure 5. The FTIR spectra of $Se_{90}Ge_{10}$, $Se_{80}Ge_{20}$ and $Se_{70}Ge_{30}$ as-prepared samples

1- The bonding nature: The structural investigations of Ge-Se alloys according to Raman spectra (Fig. 3) showed that the structure of glassy phase in $GeSe_2$-Se subsystem consists of Se_8 puckered rings, Se_n spiral chains as well as $Ge(Se_{1/2})_4$ tetrahedral and $Ge_2(Se_{1/2})_6$ ethane like in proportions varying to comply with the actual x-values [13-17]. In fact, strong covalent bonds exist between the Se-Se atoms in the Se_n chains and Se_8 rings, whereas between the chains and rings there is weak Vander Waals type bonds [18]. It seems that the weak Vander Waals type bond in $GeSe_2$-Se subsystem is the main reason of low IR transmittance of fully bulk amorphous $Se_{90}Ge_{10}$ and $Se_{80}Ge_{20}$ samples. So, the

alloys in $GeSe_2$-Se subsystem are not suitable to be used in infrared windows unless the network connectivity get increased and Vander Waals type bonds be converted to strong covalent bonds. It was found that [14] by increasing the Ge content and moving to GeSe-$GeSe_2$ subsystem, the Se-Se chains and rings are vanished completely and one network with best Se-Ge connectivity ($Ge(Se_{1/2})_4$, $Ge_2(Se_{1/2})_6$ and $Ge(Se_{1/2})_2$) is formed.

2- Presence of lone pair of electrons: The absorption phenomena in chalcogenide glasses can also be due to the excitation of non-bonding (lone pair) electrons in atomic structure. The lone pair electrons of selenium in Se_8 puckered rings and Se_n spiral chains have higher energy than bonding electrons and are more excitable [19]. By attention to this point, the presence of lone pair electrons (which are absorber) in Se-rich chalcogenide glasses has destructive effect on transmittance in infrared region. This behavior was also reported by Kumar et al. [20] for $Se_{74}Sn_8Pb_{18-x}Ge_x$ (x= 7, 8, 9, 10, 11) system.

3.2. $GeSe_2$-GeSe subsystem

The XRD patterns of $Se_{60}Ge_{40}$ and $Se_{50}Ge_{50}$ bulk samples are presented in Fig. 6. According to this figure, the microstructure of $Se_{60}Ge_{40}$ as-prepared sample, which is near to eutectic reaction in $GeSe_2$-GeSe subsystem, is fully amorphous and there is not any evidence of crystalline phase in this sample. The glass transition temperature of this glass was estimated as about 331°C (Fig. 7) which is near to other reports [7]. Beside the $Se_{60}Ge_{40}$ system, the amorphous phase has not been formed in $Se_{50}Ge_{50}$ as-prepared alloy and the structure of this sample only consists of GeSe crystalline compound. The GeSe is stable compound in equilibrium phase diagram and has an orthorhombic (space group Pbnm) unit cell with a = 4.388 Å, b = 10.825 Å, and c = 3.833 Å.

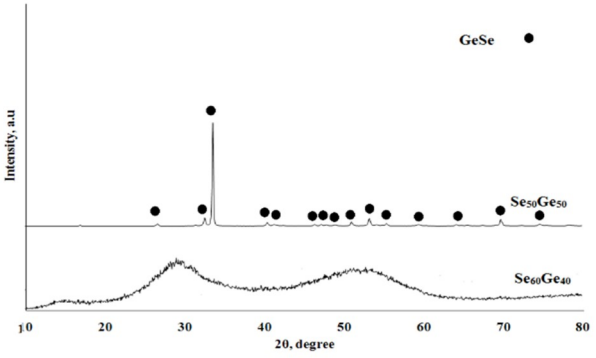

Figure 6. The XRD patterns of $Se_{60}Ge_{40}$ and $Se_{50}Ge_{50}$ as-prepared samples

In fact, higher glass forming ability of $Se_{60}Ge_{40}$ alloy in comparison with $Se_{50}Ge_{50}$ and $Se_{70}Ge_{30}$ can be attributed to the reduced glass transition temperature. The liquids temperature of eutectic composition is lower than the peritectic composition. So, the alloys with composition near to eutectic composition ($Se_{60}Ge_{40}$) have higher reduced glass transition temperature as well as glass forming ability in comparison with peritectic composition ($Se_{50}Ge_{50}$ and $Se_{70}Ge_{30}$).

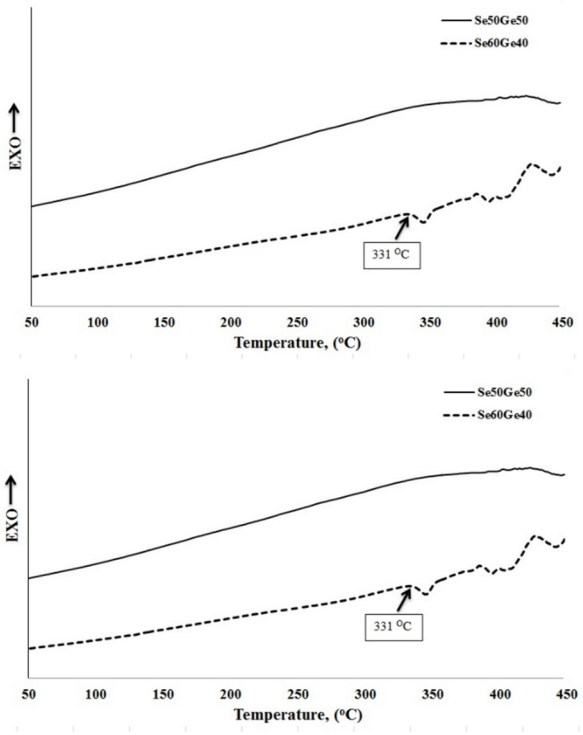

Figure 7. The DSC heating trace of $Se_{60}Ge_{40}$ and $Se_{50}Ge_{50}$ as-prepared samples in heating rate of 10°C/min

The FTIR spectra of $Se_{60}Ge_{40}$ and $Se_{50}Ge_{50}$ samples are presented in Fig. 8. According to this figure two points can be drawn as:

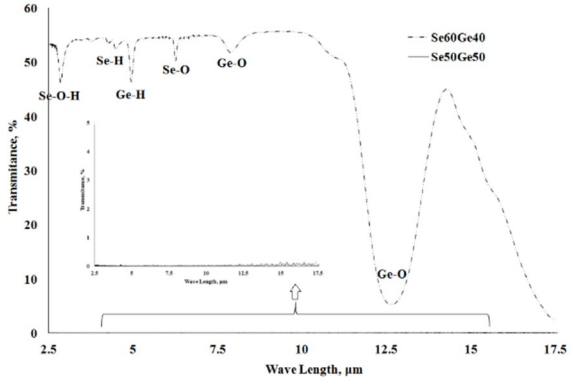

Figure 8. The FTIR spectra of $Se_{60}Ge_{40}$ and $Se_{50}Ge_{50}$ as-prepared samples

1- Same as samples prepared in Se-$GeSe_2$ subsystem, the IR transmittance of $Se_{50}Ge_{50}$ is near to zero. In

contrast, the infrared transmittance of $Se_{60}Ge_{40}$ as-prepared sample is high and reaches about 55%. In fact, the high IR transmittance of this sample can be attributed to formation of fully amorphous phase without any weak Vander Waals type interaction and lone selenium pair electrons between Se_8 rings and Se_n-chains. Based on Raman spectra (Fig. 3), by increasing the Ge content up to 30%, the Se-Se chain bonds (with lone selenium pair electrons) [9, 21] disappear and the intensity of Se-Ge is bonds with two-fold coordination around selenium and four-fold coordination around germanium increased. It seems that, replacement of Se-Se bonding in Se_8 rings and Se_n-chains (with weak Vander Waals type interaction and lone pair electrons) is the main reason leading to high IR transmittance of the prepared glasses in $GeSe-GeSe_2$ subsystem.

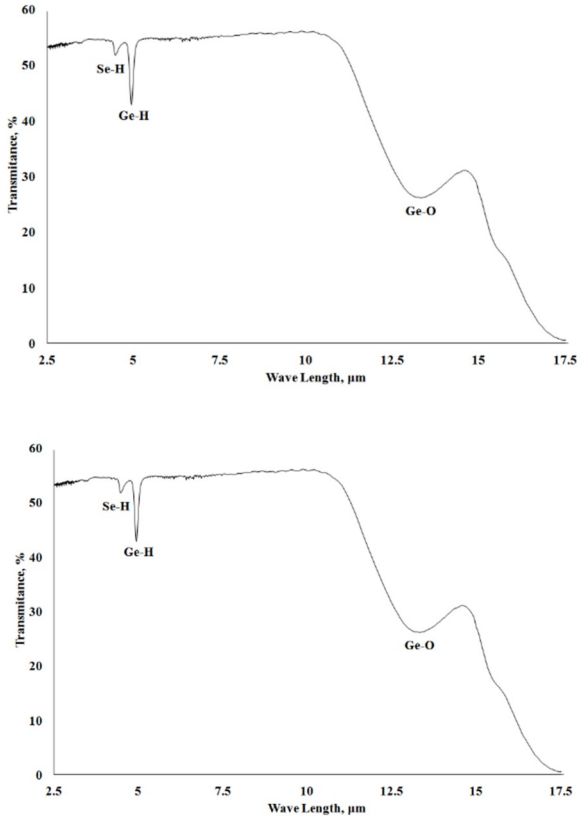

Figure 9. The FTIR spectra of $Se_{60}Ge_{40}$ as-prepared sample in presence of 100 ppm Mg

2- There are several absorption peaks at 2.85, 4.48, 4.94, 6.26, 7.9 and 12.5 µm in FTIR spectra of $Se_{60}Ge_{40}$ which are related to Se-O-H, Se-H, Ge-H, Ge-O and Ge-O, respectively [2]. As it can be seen, these peaks are attributed to oxides and hydrides impurities from raw materials and quartz ampoule. In order to remove or reduce the absorption peak intensity of oxide impurities, about 100 ppm of pure Mg element was added to the bath and the prepared sample was examined with FTIR technique. The FTIR spectrum of this sample is shown in Fig. 9. As it can be observed, addition of Mg element to $Se_{60}Ge_{40}$ has significant effects on reduction of oxide absorption bonds. It is also shown that in this condition, the Se-O-H and Se-O absorption peaks are vanished completely and the intensity of absorption peaks of Ge-O are sharply decreased. It seems that, Mg element absorbs the oxygen atoms from the melt and converts the free oxygen (Se-O and Ge-O) to bridge Mg-O-Mg bonds. In fact, this bond is so strong and do not show any absorption in IR region. However, removing the oxygen elements from Se-O-H bonds leads to increasing the intensity of absorption bands corresponding to Se-H and Ge-H, as shown in Fig. 9.

The values of refractive index of the prepared $Se_{60}Ge_{40}$ glass as a function of wavelength (determined by IR-VASE) are presented in Fig. 10. Based on this figure, two main points can be drawn:

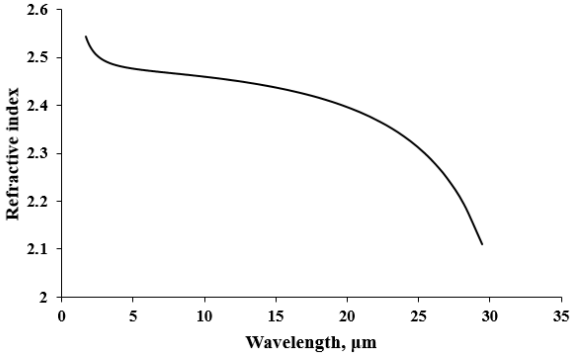

Figure 10. The calculated refraction index of $Se_{60}Ge_{40}$ glass as a function of wavelength

1- As it can be seen, the refractive index of this sample is in the range of 2.0 to 2.6. This values of refractive index are in the range of refractive index for Ge_xSe_{1-x} ($0<x<0.42$) glasses [22].

2- Regardless to the chemical composition, the refractive index of this glass is decreased with increasing the wavelength. This result is in agreement with Cauchy relation [23]:

$$n^2(\lambda) = A + \frac{B}{\lambda^2} + \frac{C}{\lambda^4} \quad (1)$$

where A, B and C are the Cauchy coefficients, which are characteristics of the material.

The UV-Visible spectrum of $Se_{60}Ge_{40}$ glass is presented in Fig. 11. As it can be seen, the absorption edge of short wavelength in UV-Visible spectra is about 950 nm. The strong absorption of this glass shows that, the extinction coefficient (K) obeys the Fermi-Dirac distribution function. Thus, the Fermi energy level can be calculated by applying Eq. 2 [24]:

$$K = \frac{1}{1+\exp[(E_F - E)/K_B T]} \quad (2)$$

where E_F is the Fermi energy, E is the variable photon energy probing the sample, K_B is the Boltzmann constant and T is the ambient temperature (297 K). In this regard, the Fermi energy of $Se_{60}Ge_{40}$ glass can be calculated by linear fitting from equation 2.

For amorphous materials, the absorption coefficient exhibits a sharp increase just before the band gap. The relation between absorption coefficient and the incident photon energy is given by Davis and Mott [25] relation:

$$a = \beta^2 \frac{(h\upsilon - E_g^{opt})^n}{h\upsilon} \quad (3)$$

where β is a constant related to the extent of the band tailing, n is the index which can have different values of 2, 3, 1/2 and 1/3 corresponding to indirect allowed, indirect forbidden, direct allowed and direct forbidden transitions, respectively. Therefore, by plotting $(\alpha h\upsilon)^{1/n}$ vs. photon energy (Tauc's plots), the intercept of the obtained line divided by slope, is equal to the energy band gap of optical transitions.

Moreover, the optical absorption in amorphous semiconductors near the absorption edge is usually characterized by three types of optical transitions corresponding to transitions between tail and tail states, tail and extended states, and extended and extended states. The first two types correspond to $h\nu \leq E_g^{opt}$ and the third one corresponds to $h\nu \geq E_g^{opt}$. Thus, the plot of absorption coefficient versus photon energy (α vs. hν) has three different regions. In the second region, the absorptions is related to transitions from the localized tail states above the valence band edge to extended states in the conduction band and/or from extended states in the valence band to localized tail states below the conduction band. The spectral dependence of absorption coefficient usually follows the so-called Urbach rule:

$$\alpha = \beta \exp(\frac{h\upsilon}{E_U}) \quad (4)$$

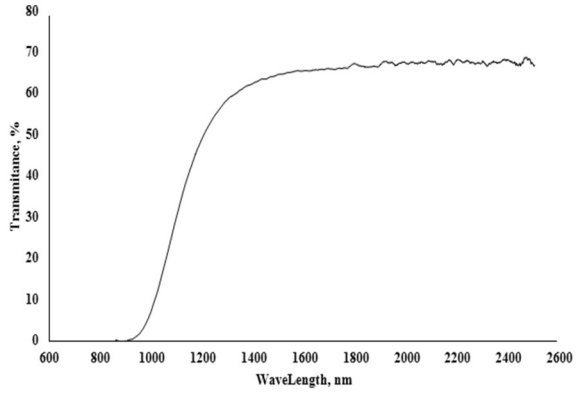

Figure 11. The UV-Visible spectra of $Se_{60}Ge_{40}$ as-prepared sample in presence of 100 ppm Mg

By attention to these equation, and linear fitting of Ln α against hν curves in the tailing part of localized states [26], the Urbach energy (E_U) can be calculated.

Based on above equations, the Fermi energy, direct and indirect allowed optical band gaps and Urbach energy of $Se_{60}Ge_{40}$ glass were calculated and the obtained results are presented in Table 2. These results are near to optical properties of $Se_{0.62}Ge_{0.38}$ with direct band gap, indirect band gap and Urbach energy equal to 1.79, 1.81 and 0.26 eV, respectively [27].

TABLE 2. Fermi energy, direct and indirect allowed optical band gaps and Urbach energy of $Se_{60}Ge_{40}$ glass

Fermi energy (eV)	Urbach energy (eV)	Indirect band gap (eV)	Direct band gap (eV)
0.3879	0.1526	1.345	1.28

4. CONCLUSION

In this study, the structural and optical characterization of $Se_{100-x}Ge_x$ alloying system during melt quenching process was investigated. The results showed that the glass forming ability of $Se_{70}Ge_{30}$ and $Se_{50}Ge_{50}$ is so low and the structures of these alloys after quenching are combination of amorphous, GeSe and Ge_3Se_7 compounds. Although the structures of the as-prepared $Se_{90}Ge_{10}$, $Se_{80}Ge_{20}$ and $Se_{60}Ge_{40}$ are fully amorphous, only $Se_{60}Ge_{40}$ shows IR transmittance. The refractive index of this glass is in the range of 2.0 to 2.6 and it was decreased with increasing the wavelength. The absorption edge of short wavelength in UV-Visible spectra for $Se_{60}Ge_{40}$ is about 950 nm. Addition of Mg element (100 ppm) has the best effect on removing the oxide impurity bonds in IR spectrum.

5-ACKNOWLEDGMENTS

The authors like to thank Mr. A. Rahimian and Mr. M. Rezazadeh for their collaborations in experiments.

REFERENCES

1. Zhang, X.H., Guimond, Y. and Bellec, Y.,"Production of complex chalcogenide glass optics by molding for thermal imaging", ***Non-Crystalline Solids***, Vol. 326-327, (2003), 519-523.
2. Shiryaev, V.S., Ketkova, L.A., Churbanov, M.F., Potapov, A.M., Troles, J., Houizot, P., Adam, J.L. and Sibirkin, A.A., "Heterophase inclusions and dissolved impurities in $Ge_{25}Sb_{10}S_{65}$ glass", ***Physics and Chemistry of Solids***, Vol. 335, (2009), 2640–2646.
3. Philips, J.C., "Topology of covalent non-crystalline solids III: kinetic model of the glass transition", ***Non-Crystalline Solids***, Vol. 44, (1981), 17-30.
4. Fawcett, R.W., Wagner, C.N.J. and Cargill, G.S., "Radial distribution studies of amorphous GexSe1-x alloy films", ***Non-Crystalline Solids,*** Vol. 8-10, (1972), 369-375.

5. Kauzmann, W., "The nature of the glassy state and the behavior of liquids at low temperatures", ***Chemical Reviews,*** Vol. 43, No. 2, (1948), 219-256.
6. Turnbull, D., "Under what conditions can a glass be formed", ***Contemporary Physics Publishing,*** Vol. 10, (1969), 473-488.
7. Isper, H., Gambino, M. and Schuster, W., "The Germanium-Selenium phase diagram", ***Chemical Monthly***, Vol. 113, (1982), 389-398.
8. Guin, J. and Rouxel, T., "Indentation creep of Ge-Se chalcogenide glasses below Tg: elastic recovery and non-Newtonian flow", ***Non-Crystalline Solids***, Vol. 298, (2002), 260-269.
9. Kawamura, H. and Matsumura, M., "Spectroscopic studies of the structure of amorphous Se-Ge", ***Non-Crystalline Solids***, Vol. 35, (1980), 1215-1220.
10. Adam, J.L. and Zhang, X., "Chalcogenide glasses preparation, properties and applications", Woodhead Publishing, USA and New Delhi, (2014), 36- 48, 347- 380.
11. Popescu, M., "Disordered chalcogenide optoelectronic materials: phenomena and applications", ***Optoelectronics and Advanced Materials***, Vol. 7, (2005), 2189–2210.
12. Stolen, S., Johnsen, H.B., Boe, C.S., Grande, T. and Karlsen, O.B., "Stable and metastable phase equilibria in the $GeSe_2$-Se system", ***Phase Equilibria,*** Vol. 20, (1999), 17-28.
13. Savage, J.A. and Hilger, A., "Infrared optical materials and their antireflection coatings", Optics and laser technology, (1985).
14. Sharma, P. and Katyal, S.C., "Far-infrared transmission and bonding arrangement in $Ge_{10}Se_{90-x}Te_x$ semiconducting glassy alloys", ***Non-Crystalline Solids***, Vol. 354, (2008), 3836–3839.
15. Wei, W.H., Wang, R.P., Shen, X., Fang, L. and Luther-Davies, B., "Correlation between structural and physical properties in Ge–Sb–Se glasses", ***Physics Chemistry C***, Vol. 117, (2013), 16571–16576.
16. Qiao, B., Dai, S., Xu, Y., Zhang, P., Shen, X., Xu, T., Nie, Q., Ji, W. and Chen, F., "Third-order optical nonlinearities of chalcogenide glasses within Ge-Sn-Se ternary system at a mid-infrared window", ***Optical Materials Express***, Vol. 5, (2015), 2359-2365.
17. Ghayebloo, M., Tavoosi, M. and Rezvani, M., "Compositional Modification of Se-Ge-Sb Chalcogenide Glasses by addition of Arsenic Element", ***Infrared Physics and Technology***, Vol. 83, (2017), 62-67.
18. Lafi, O.A. and Imran, M.M.A., "Compositional dependence of thermal stability, glass-forming ability and fragility index in some Se–Te–Sn glasses", ***Alloys and Compounds***, Vol. 509, (2011), 5090–5094.
19. Delaizir, G. and Calvez, L., "A novel approach to develop chalcogenide glasses and glass-ceramics by pulsed current electrical sintering (PCES), Sintering of Ceramics – New Emerging Techniques", ***Publishing Process Manager Sasa Leporic,*** (2012), 281-306.
20. Kumar, P., Modgil, V. and Rangra, V.S.,"The characterization and study of physical parameters of Ge modified Se-Sn-Pb chalcogenide system", ***Glass and Ceramics***, Vol. 3, (2013), 116-121.
21. Aly, K.A., Abd Elnaeim, A.M., Afify, N. and Abousehly, A.M., "Improvement of the electrical properties of Se_3Te1 thin films by in additions", ***Non-Crystalline Solids,*** Vol. 358, (2012), 2759–2763.
22. Yang, G., Gueguen, Y., Sangleboeuf, J.-C., Rouxel, T., Boussard-Plédelb, C., Troles, J., Lucas, P. and Bureau, B., "Physical properties of the $GexSe_{1-x}$ glasses in the 0bxb0.42 range in correlation with their structure", ***Non-Crystalline Solids,*** Vol. 377, (2013), 54–59.
23. Li, J. and Wu, S., "Extended Cauchy equations for the refractive indices of liquid crystals", ***Applied physics***, Vol. 95, No. 3, (2004), 896-901.
24. Rezvani, M. and Farahinia, L., "Structure and optical band gap study of transparent oxyfluoride glass-ceramics containing CaF2 nanocrystals", ***Materials and Design,*** Vol. 88, (2015), 252–257.
25. Mott, N.F. and Davis, E.A., "Electronic processes in nanocrystalline materials", Clarendon press, Oxford, (1971).
26. Rani, S., Sanghi, S., Agarwal, A. and Seth, V.P., "Study of optical band gap and FTIR spectroscopy of $Li_2O{\cdot}Bi_2O_3{\cdot}P_2O_5$ glasses", ***Spectrochim. Acta A,*** Vol. 74, (2009), 673–677.
27. Fadel, M., Fayek, S.A., Abou-Helal, M.O., Ibrahim, M.M. and Shakra, A.M., "Structural and optical properties of SeGe and SeGeX (X = In, Sb and Bi) amorphous films", ***Alloys and Compounds***, Vol. 485, (2009), 604–609.